

Use of light absorbers to alter optical interrogation with epi-illumination and transillumination in three-dimensional cardiac models

Venkat K. Ramshesh

Stephen B. Knisley

The University of North Carolina at Chapel Hill
Department of Biomedical Engineering
CB# 7575, 152 MacNider Hall
Chapel Hill, North Carolina 27599-7575
E-mail: sknisley@email.unc.edu

Abstract. Cardiac optical mapping currently provides 2-D maps of transmembrane voltage-sensitive fluorescence localized near the tissue surface. Methods for interrogation at different depths are required for studies of arrhythmias and the effects of defibrillation shocks in 3-D cardiac tissue. We model the effects of coloadng with a dye that absorbs excitation or fluorescence light on the radius and depth of the interrogated region with specific illumination and collection techniques. Results indicate radii and depths of interrogation are larger for transillumination versus epi-illumination, an effect that is more pronounced for broad-field excitation versus laser scanner. Coloadng with a fluorescence absorber lessens interrogated depth for epi-illumination and increases it for transillumination, which is confirmed with measurements using transillumination of heart tissue slices. Coloadng with an absorber of excitation light consistently decreases the interrogated depths. Transillumination and coloadng also decrease the intensities of collected fluorescence. Thus, localization can be modified with wavelength-specific absorbers at the expense of a reduction in fluorescence intensity. © 2006 Society of Photo-Optical Instrumentation Engineers. [DOI: 10.1117/1.2187012]

Keywords: optical mapping; transmembrane voltage; epi-illumination; transillumination; Monte Carlo model; heart.

Paper 05305R received Oct. 10, 2005; revised manuscript received Dec. 21, 2005; accepted for publication Dec. 29, 2005; published online Mar. 23, 2006.

1 Introduction

Optical methods with transmembrane voltage-sensitive fluorescent dyes enable simultaneous multisite mapping of transmembrane potentials in the heart. This is advantageous over intracellular microelectrodes, which are usually limited to a single site at a given time.¹⁻⁵ In cardiac optical mapping, excitation light is directed onto a heart stained with a voltage-sensitive fluorescent dye, while the fluorescence that exits the heart surface is collected. The mapping is performed with either epi-illumination, in which the light source and collector are aimed at the same surface of the tissue being mapped, or transillumination, in which the light source and collector are aimed at opposite surfaces.³ Most cardiac mapping systems illuminate a broad area of the tissue surface while imaging the surface with a CCD or photodiode array (broad-field excitation method). This achieves localization for each measurement site by allowing only photons that exit a small region of the cardiac surface to enter each element of the array. It is also possible to achieve localization by controlling the area of the excitation light with a scanned laser beam while collecting fluorescence photons that exit a large tissue surface area with a photomultiplier tube⁶ (laser scanner excitation method). In

this case, the excitation beam is located at only one spot at an instant in time. The fluorescence collected then represents only the effects produced by the beam at that location.⁴

For epi-illumination, the optical maps are 2-D and represent fluorescence that originates within less than approximately 0.1 cm from the illuminated tissue surface.⁴ This has limited the ability to examine events such as ventricular fibrillation and electrical defibrillation shocks for which the transmembrane potential distributions throughout the ventricular wall are important. To overcome this, transillumination of cardiac tissue was developed for the broad-field excitation method. With transillumination, Baxter et al. showed the collected fluorescence originates deeper within cardiac tissue compared with that for epi-illumination.³

The paper by Baxter et al. also presents a 1-D exponential model that predicts that the depth of interrogation for transillumination depends on decay constants of the excitation and fluorescence.³ We further hypothesized that coloadng with an additional dye that is nonfluorescent and not voltage sensitive but absorbs light at an excitation or fluorescence wavelength will decrease or increase, respectively, the interrogated depth for transillumination. The coloadng may also affect the width of the tissue interrogated. However, quantitation of the size of the tissue region interrogated requires a model that incorporates scattering in 3-D tissue. We did not find a report of the

Address all correspondence to Stephen Knisley, Biomedical Engineering, Univ. of North Carolina/Chapel Hill, 152 Macnider Hall – CB 7575, Chapel Hill, NC 27599. Tel: 919-966-6653. Fax: 919-966-2963. E-mail: sknisley@email.unc.edu

depth of interrogation with transillumination for the laser scanner excitation method, the radius of interrogation with transillumination for any method, or the quantitative changes in interrogated depth or radius produced by coloaded with an absorbing dye for any method.

Here, we examine sizes of interrogated regions using Monte Carlo models that incorporate 3-D scattering and absorption of light in cardiac tissue. We examined epi- and transillumination for both the broad-field and the laser scanner excitation methods. For each of these, we determined whether the addition of absorbing dyes may produce a desired effect on interrogated depth. This was done in separate simulations by varying the absorption coefficients for light at excitation and fluorescence wavelengths from their nominal values previously measured in dye-stained cardiac tissue.

The results show that addition of an excitation light absorber lessened depth of interrogation for all methods examined. Addition of a fluorescence absorber increased the depth of interrogation for transillumination, which was confirmed with experiments using heart tissue slices. Also the lateral extent of interrogation was altered by the addition of an absorber, an effect that was most pronounced for the transillumination with broad-field excitation. However, the collected fluorescence intensity decreased with transillumination and with the addition of an absorber. Thus, epi-illumination or transillumination can be used with absorbers to modify interrogated regions at the expense of signal intensity.

2 Methods

We used Monte Carlo models similar to the model developed by Wang et al. to simulate the propagation of excitation and fluorescence light inside the tissue.⁷ While the methods were described in an earlier paper,⁸ a brief description follows. Figure 1(a) illustrates the tissue arrangement used in our simulations. The 0.25-cm-thick tissue was assumed to be homogeneous, which meant that every part of the tissue had the same absorption coefficient, scattering coefficient, scattering anisotropy, and refractive index. The models launched photons and simulated their propagation inside tissue.⁷ Photons were treated as classical particles, having no specific phase or polarization. Three different coordinate systems were used to launch and propagate photons inside the tissue [Fig. 1(b)]. A Cartesian coordinate system in three dimensions was used to track photon movements. The xy plane represented the illuminated tissue surface and the z direction represented depth normal to the surface. The recording of photon absorption in the tissue was done in a cylindrical coordinate system given by r , Θ , and z , which provided radial and depth coordinates for the distribution of fluence. The z coordinate of the cylindrical system was shared with the Cartesian coordinate system. A spherical coordinate system whose z axis was dynamically aligned with the photon propagation direction was used to sample the change in photon propagation direction due to each scattering event. This system was described by the deflection angle ψ and azimuthal angle ϕ .

After a photon was launched, a step size, i.e., distance traveled during each step, was determined for the photon probabilistically, based on the absorption and scattering coefficients of the tissue. The step size was determined using the following equation⁷

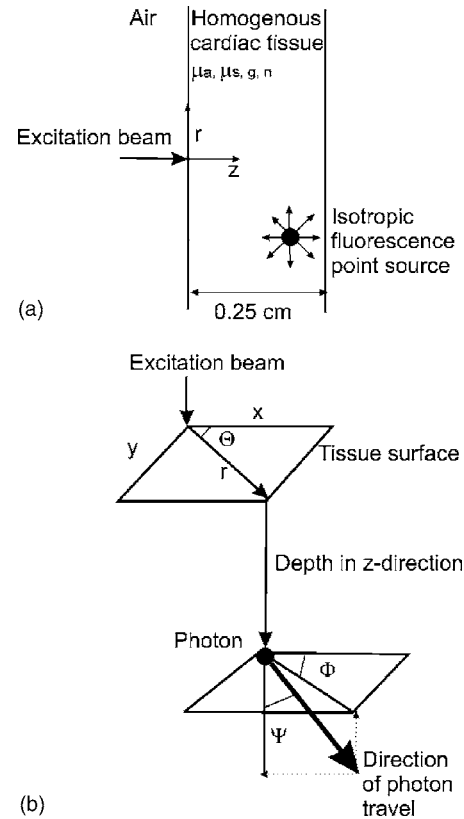


Fig. 1 Cardiac tissue arrangement and coordinate systems used in the simulations showing: (a) tissue surfaces and dimensions and (b) coordinate systems for photon propagation and recording. The tissue had a thickness of 0.25 cm (z direction), while the radius (r) was unlimited for propagation of excitation and fluorescent photons.

$$\text{step size} = -\ln(\xi)/(\mu_a + \mu_s), \quad (1)$$

where ξ is a random number from 0 to 1, μ_a is the tissue absorption coefficient, and μ_s is the tissue scattering coefficient. The program then determined whether the photon hit a surface of the tissue. If it did not hit a surface, the photon moved to a new location inside the tissue based on its step size and current propagation direction. The coordinates of the photon at the new location in the Cartesian system were given by

$$\begin{aligned} x_{\text{new}} &= x + \mu_x, \\ y_{\text{new}} &= y + \mu_y, \\ z_{\text{new}} &= z + \mu_z, \end{aligned} \quad (2)$$

where μ_x , μ_y , and μ_z are the direction cosines in the x , y , and z directions, respectively. At new locations of the photon, part of the photon weight (w) was absorbed and recorded and the remaining part scattered.

$$w_{\text{abs}} = w(\mu_a/\mu_t), \quad (3)$$

where w_{abs} is the weight absorbed, and μ_t is the sum $\mu_a + \mu_s$.

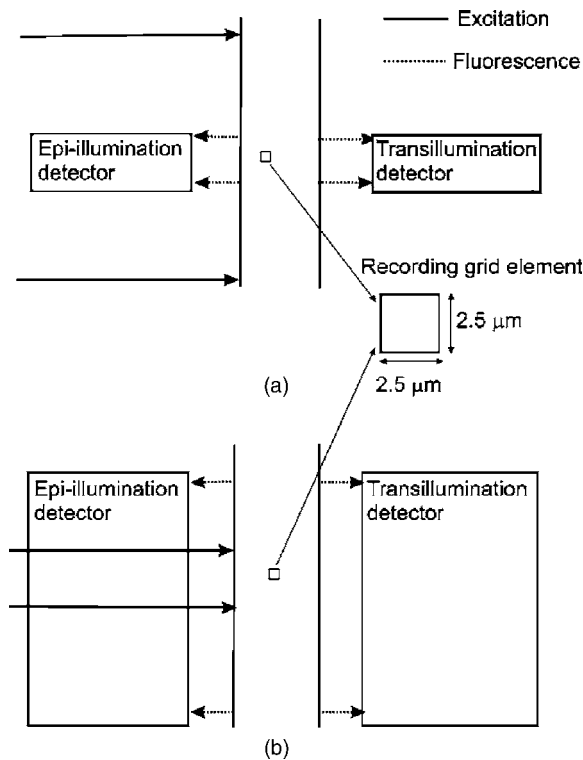


Fig. 2 Diagrams of simulated excitation and collection methods: (a) broad-field excitation and (b) laser scanner excitation. The maximum illumination radius (solid horizontal arrows directed onto tissue from left) was larger for the broad-field excitation. The fluence was recorded using a cylindrical coordinate system and grids with depth and radial increments of $2.5 \mu\text{m}$ (single grid element shown). Fluorescent photons that escaped the tissue within a narrow radius at the illuminated or opposite tissue surface (maximum radius indicated with dotted arrows) were collected for broad-field excitation. All fluorescence photons that escaped a surface were collected for the laser scanner excitation. Escaping fluorescence photons had variable directions of travel (not shown).

Propagation of the photon continued with a new step size [calculated using Eq. (1)] until the weight (w) of the photon fell below a threshold or it hit a surface. If its weight fell below a threshold, the photon had a probability of $1/m$ to survive with an updated weight of mw and continue propagation. This technique avoided the energy conservation rule violation that would occur if photon packets falling below the threshold weight were simply terminated.⁷ If a photon hit a surface it either reflected back into the tissue or exited from the tissue, depending on its current direction of propagation and the refractive index of the tissue. In these simulations, a photon could continue to propagate and reach any radius until it was absorbed or exited a surface of the tissue.

2.1 Excitation Simulation

Simulations of the excitation light at 488 nm were performed with an illumination radius of 0.1 cm for the laser scanner excitation and 0.5 cm for the broad-field excitation method. Illumination was uniform within a circular area. Figure 2 shows the different excitation and collection methods used. The fluence produced by a radial section containing 200 beams normal to the tissue surface was expressed with a ho-

mogenous grid system in radial and depth coordinates (i.e., the grid was constructed with uniform increments in the coordinates). All results presented used a grid with increments of $2.5 \mu\text{m}$. We used 1000 elements in the depth direction to represent a tissue thickness of 0.25 cm, which is comparable to ventricular free wall thicknesses in rabbit hearts. For each depth, the excitation fluence values were recorded at all grid elements within a radius of 0.25 cm. Contours of the normalized excitation fluence in the tissue did not change when we repeated a simulation with 1×10^6 , 2×10^6 , and 3×10^6 incident photons in the radial section. In all results presented, the excitation simulations used 2×10^6 incident photons, which corresponded to energy densities of 26 and $1 \text{ pJ}/\text{cm}^2$ for the laser and broad-field excitation methods, respectively. Simulations used the values for absorption coefficient ($\mu_a = 5.2/\text{cm}$), scattering coefficient ($\mu_s = 232/\text{cm}$), and scattering anisotropy ($g = 0.94$) that were previously measured for a light wavelength of 488 nm in heart tissue stained with the transmembrane voltage-sensitive dye,⁶ di-4-ANEPPS. In additional simulations, the scattering and anisotropy properties were held constant while the absorption coefficient at 488 nm was changed from the measured value of 5.2/cm to 1.8, 15.6, and 52/cm. This indicated the effects of 1/3-, 3-, and 10-fold changes in absorption coefficient of excitation light.

2.2 Fluorescence Simulation

To study the fluorescence propagation, simulations were performed with optical properties of tissue for light at a wavelength of 669 nm. During fluorescence simulations each grid element within the recording radius was regarded as a point source from which fluorescence originated. The weight assigned to fluorescence photons launched at each element was directly proportional to the fluence of the excitation light to represent fluorescence produced by the single-photon excitation process.⁹ The initial direction of travel of launched fluorescence photons was isotropic [i.e., the direction was determined randomly with all directions having the same probability, Fig. 1(a)].

In pilot simulations, we launched one fluorescence photon at each element. To lessen irregularities in contours of the interrogated regions, we also performed simulations in which the number of launched fluorescence photons was increased to 10, 100, and finally 1000 per element. The increases from 1 to 100 improved smoothness of contours. However, results were similar when the number was increased from 100 to 1000. All results presented used 1000 photons launched per element.

We selected 669 nm to represent fluorescence because this is near^{10,11} the wavelength of peak fluorescence emitted from the transmembrane voltage-sensitive dye di-4-ANEPPS. Also, values of the optical properties at this wavelength ($\mu_a = 1.0/\text{cm}$, $\mu_s = 218/\text{cm}$, $g = 0.96$) have been measured⁶ in heart tissue stained with di-4-ANEPPS. In different simulations, the scattering and anisotropy properties were held constant while the absorption coefficient at 669 nm was changed from the measured value of 1/cm to 0.3, 3, and 10/cm. This indicated the effects of 1/3-, 3-, and 10-fold changes in absorption of fluorescence.

During fluorescence simulations, weights of fluorescence photons that exited each of the surfaces (epi- and transillumination, respectively) of the tissue and the locations of their

origin inside the tissue were saved in memory. For simulations of the laser scanner excitation method, all photons exiting a given surface were collected to represent the large collection area of a photomultiplier tube.⁴ For simulations of the broad-field excitation method, only the photons exiting a given surface within a radius of 0.05, 0.1, or 0.25 cm were collected. We chose to show the results for the 0.1-cm exit radius because this is comparable to the size of a photodiode array element used in mapping with broad-field excitation.²

We used locations of the origin of collected fluorescence photons to evaluate the interrogated region, defined as the specific region in radial and depth coordinates inside the tissue from which a given percentage of the total collected fluorescence originated.^{6,8}

Our analysis determined interrogated regions based on fractions of the total collected fluorescence so that the size of the regions was independent of factors that alter fluorescence yield such as concentration of fluorescent dye. This was confirmed by similarity of interrogated regions (except for noise) when simulations were repeated with different numbers of launched fluorescence photons at each element. To reduce effects of random noise, all results shown were spatially smoothed by binning fluorescence contributions from 40×40 neighboring grid elements, which resulted in plots of interrogated regions with $100\text{-}\mu\text{m}$ resolution.

2.3 Applicability to Multisite Cardiac Optical Mapping

Our simulations with the laser excitation method used a single laser beam to predict the interrogated region, while in cardiac optical mapping experiments the laser beam scans sequentially to multiple sites.⁴ During laser scanning of the heart with 128 spots at a sampling rate of 1 kHz for each spot as performed in our laboratory, samples of light corresponding to consecutive spots were collected $7.8\ \mu\text{s}$ apart in time. However, the propagation and absorption of laser photons and the production of fluorescence at a given spot takes only a few nanoseconds. For example, Delpy et al.¹² have shown the largest transit time for a photon to propagate through a 1-cm slab of brain tissue ($\mu_a=0.456/\text{cm}$ and $\mu_s=60/\text{cm}$) is approximately 0.5 ns. Given this difference in time scales, the fluorescence produced by illumination at one spot will be unaffected by the illumination at other spots during scanning. Thus, we determined the size of the interrogated region for a single beam centered on the z axis. We considered that the origin of a cylindrical coordinate system can be placed at any arbitrary location on the heart surface, so the size that we found in the simulation may apply to any location of the beam that occurs during scanning. Lateral movement of the laser beam to a different spot during scanning of the tissue produces corresponding movement of the interrogated region.

Similarly, our simulations with the broad-field excitation method use a single imaged site on a tissue surface from which fluorescence can be projected to an imaging array element to predict the size of the interrogated region. In cardiac optical mapping experiments, fluorescence photons from multiple imaged sites are projected to corresponding array elements. However, given that the origin of the model can be located arbitrarily, the size of the interrogated region may still apply to any imaged site on the tissue surface. Also the fact

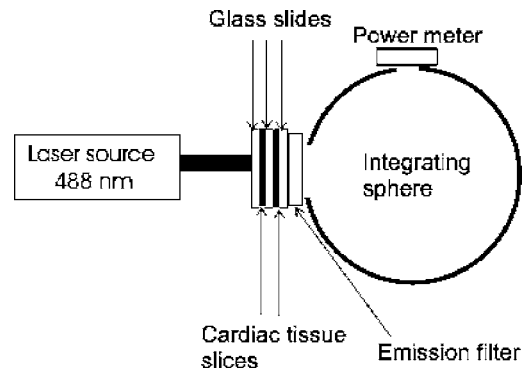


Fig. 3 Schematic of setup for the experimental measurements. A laser beam (488 nm) of approximately 0.3 cm diameter illuminated a pair of 0.1-cm-thick cardiac tissue slices held between glass slides. Fluorescence light escaping the opposite surface of the tissue slices passed through a 530-nm longpass or $670\pm 6\text{-nm}$ bandpass emission filter into an integrating sphere (24.5 cm diameter) and was measured with a power meter.

that illumination is simultaneous over a large surface area is taken into account in the simulations of the broad-field excitation method.

2.4 Experimental Measurements

We performed experimental measurements with pairs of 0.1-cm-thick rabbit cardiac slices between glass slides. Three experiments were performed using slices from three hearts. Each experiment included a control pair and a pair stained with a fluorescence absorber.

Figure 3 shows a schematic of the experimental setup. Experiments determined relative contributions of tissue at different depths to the signal measured with transillumination, and whether these contributions are altered by an increase in fluorescence absorption. Control pairs consisted of a slice stained with di-4-ANEPPS (15 min immersion in a solution containing 2 mL of di-4-ANEPPS-saturated ETOH in 100 mL water) and a nonstained slice. We oriented the tissue so that the stained slice was either near or far from the illuminated surface (i.e., shallow or deep). Since dye fluorescence may only originate in the stained slice, fluorescence measurements for the two orientations indicated approximate contributions of shallow and deep tissue.

The tissue was illuminated with an approximately 0.3-cm-diam beam from an argon laser (Lexel 95, 488 nm, 40 to 80 mW). Fluorescence exiting the far side of the tissue passed through a longpass (wavelengths $>530\ \text{nm}$) or bandpass filter ($670\pm 6\ \text{nm}$) into an integrating sphere (Labsphere, 24.5-cm diameter). The longpass filter enabled us to collect light from a large portion of the fluorescence spectrum, whereas the bandpass filter provided measurements directly applicable to the fluorescence wavelength of 669 nm used in our Monte Carlo simulations. A power meter (Newport 840 with 4031 probe) attached to the sphere indicated transillumination-induced fluorescence intensity.

To examine the effect of increased red absorption, pairs of slices were initially stained with a fluorescence absorber (Signature Brand, blue 1, 0.3 g in 100 mL water), which produced visible darkening of specimens. One of the slices in

each of these pairs was then stained with the di-4-ANEPPS. Measurements of the transillumination-induced fluorescence intensity were performed for the two orientations.

3 Results

In Figs. 4–7, the tissue was illuminated by excitation light from the left side of the figure. Emitted fluorescence was collected from the left side for epi-illumination, and the right side for transillumination.

3.1 Interrogated Region with Normal Optical Properties of Stained Hearts

Figures 4(a) and 4(d) show the interrogated regions for the broad-field excitation method with normal optical properties, i.e., the values that have been measured in di-4-ANEPPS-stained heart tissue.⁶ Figure 4(a) shows the results for epi-illumination while Fig. 4(d) shows the results for transillumination. The absorbed excitation light (total weight of excitation photons absorbed in tissue within the 0.25-cm recording radius) was 21% of the total weight of all incident excitation photons. When expressed as a percentage of the weight of just those excitation photons incident within the recording radius, the absorbed excitation light was 84%.

Depths of interrogation for all the contours were greater for transillumination than for epi-illumination. For example, at a radius of 0.05 cm, the 80% contour in Fig. 4(a) had a depth of approximately 0.1 cm, while the corresponding depth in Fig. 4(d) was 0.25 cm (i.e., it included the entire tissue thickness). The maximum radius of interrogation was greater for the transillumination, e.g., maximum radius of the 80% contour was 0.13 cm for epi-illumination and 0.21 cm for transillumination. The total weight of collected fluorescence photons for transillumination was 38% of that for epi-illumination, consistent with greater travel distance and absorption of photons for transillumination.

Figure 5 shows the contributions to the collected fluorescence from different depths at a radius of 0.01 cm for the broad-field excitation method with the normal optical properties. Contributions are expressed as percentages of the total collected fluorescence that originated from all depths at that radius. Figure 5(a) shows the results for epi-illumination, while Fig. 5(b) shows the results for transillumination. The contributions for epi-illumination rapidly decrease at all depths shown, whereas contributions for transillumination decrease gradually.

Figures 6(a) and 6(d) show interrogated regions for the laser scanner excitation method with normal optical properties. The absorbed excitation light within the recording radius was 83% of the weight of incident excitation photons. Again, depth of interrogation for all contours was greater for transillumination compared with epi-illumination [e.g., at a radius of 0.05 cm the 80% contour in Fig. 6(a) had a depth of approximately 0.1 cm, while the corresponding depth in Fig. 6(d) was 0.15 cm]. The total weight of collected fluorescence photons for transillumination was 61% of that for epi-illumination.

Figure 7 shows the contributions to the collected fluorescence from different depths at a radius of 0.01 cm for the laser scanner excitation method with the normal optical properties. As found for the broad-field excitation method, the

largest contributions to the collected fluorescence occurred from tissue at shallow depth. Also the contributions for epi-illumination decreased more rapidly with depth than occurred for transillumination (e.g., at a depth of 0.15 cm for epi-illumination the contribution decreased to 6% of the maximum contribution, whereas for transillumination the contribution decreased to 17% of the maximum). For transillumination, however, the decrease found with the laser scanner excitation method was more rapid than that with broad-field excitation method [e.g., Fig. 7(b) versus Fig. 5(b)].

The total weight of collected fluorescence expressed as a percentage of the weight of excitation photons incident on the tissue surface within the recording radius was greater with the laser scanner excitation method compared with the broad-field method. For epi-illumination, this value for the laser scanner method in Fig. 6(a) was 9 times that for the broad-field method in Fig. 4(a). For transillumination, the value in Fig. 6(d) was 14 times that in Fig. 4(d).

3.2 Effects of Altered Absorption Coefficients

Panels (b), (c), (e), and (f) in Figs. 4 and 6 show the interrogated regions when the absorption properties of the tissue at 488 or 669 nm were varied. Figure 4 shows results for the broad-field excitation method, while Fig. 6 shows results for the laser scanner excitation method. The center panels in each column show the effect of a threefold increase of the absorption coefficient of fluorescence, while the bottom panels show the effect of a threefold increase of the absorption coefficient of excitation light.

The increased fluorescence absorption coefficient produced a slight decrease in the interrogated depths for epi-illumination, e.g., at a radius of 0.05 cm, the 80% contour had a depth of approximately 0.1 cm for the normal conditions and 0.9 cm when the absorption was increased [Fig. 4(b) versus Fig. 4(a) and Fig. 6(b) versus Fig. 6(a)]. However, for transillumination the interrogated depths increased [Fig. 4(e) versus Fig. 4(d) and Fig. 6(e) versus Fig. 6(d)]. This was more pronounced for the broad-field excitation, for which the brightest collected fluorescence photons originated away from the illuminated surface [20% contour in Figure 4(e)]. Also the radius of interrogation decreased for the broad-field method.

The increased absorption coefficient of fluorescence did not affect the excitation light or its absorption in the models, however, the total weight of collected fluorescence decreased. The decreases, expressed as a percentage of the total weight of collected fluorescence for the heart tissue with normal absorption, were 25% for broad-field excitation with epi-illumination, 47% for broad-field excitation with transillumination, 43% for laser scanner excitation with epi-illumination, and 63% for laser scanner excitation with transillumination.

When we increased the absorption coefficient of the 488 nm excitation light threefold, the major effect on the interrogated regions was a decrease in the depth of interrogation, which was observed for all methods examined [panels (c) versus (a) and (f) versus (d) in Figs. 4 and 6]. The total weight of excitation photons absorbed inside the tissue increased to 93 and 94% of the excitation light incident within the recording radius (compared with the 84 and 83% described for the normal absorption with broad-field and laser scanner excitation methods, respectively). The total weight of

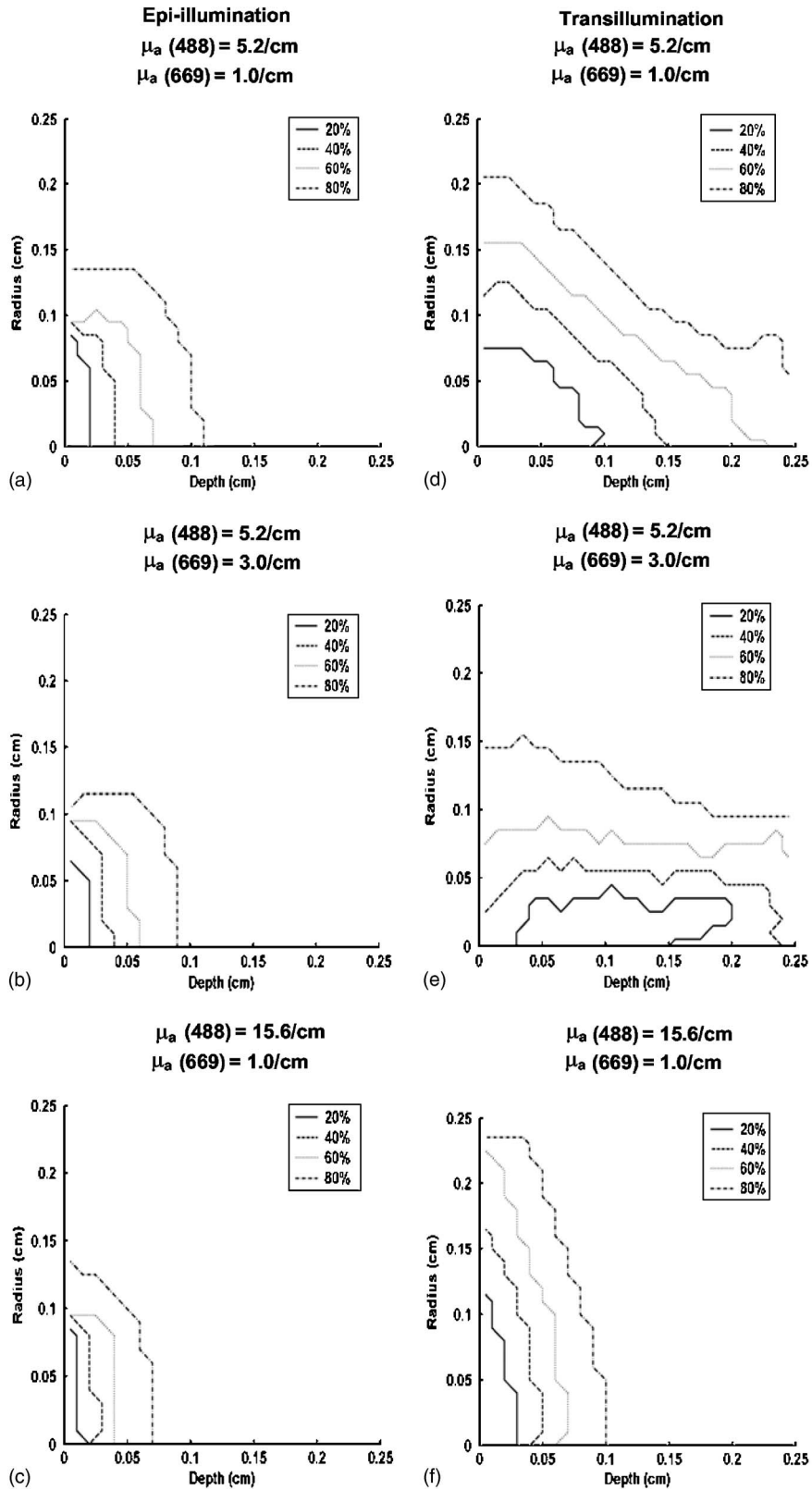


Fig. 4 Interrogated regions inside tissue for broad-field excitation method with normal and threefold increase in absorption coefficients for excitation and fluorescence light wavelengths. Illumination radius was 0.5 cm. The region enclosed by each contour contains the originating sites of the collected photons having the greatest weights and whose summed weight was 20, 40, 60, or 80% of the total for all collected photons. Left column shows results for epi-illumination: (a) plot results for normal conditions, (b) effect of threefold increase in the absorption coefficient for the fluorescent wavelength, and (c) effect of threefold increase in the absorption coefficient for the excitation wavelength. Right column shows corresponding results for transillumination.

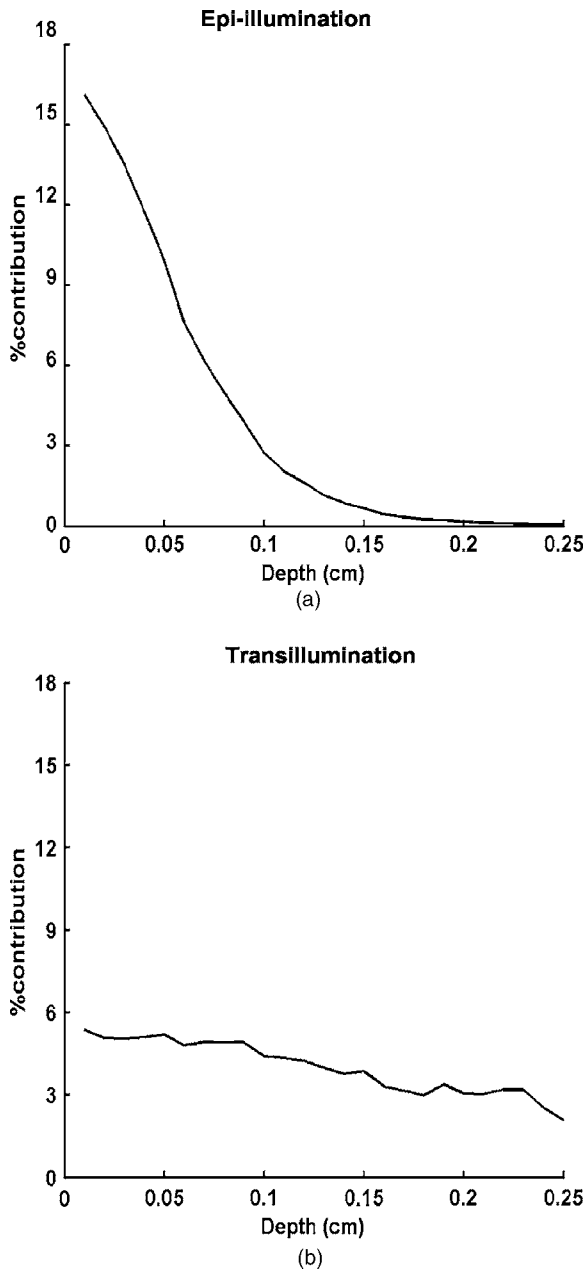


Fig. 5 Fluorescence contributions from different depths at a radius of 0.01 cm inside the tissue with normal optical properties for the broad field excitation method with results for (a) epi-illumination and (b) transillumination. The simulation was same as in Figs. 4(a) and 4(d). Fluorescence contribution from each depth was expressed as a percentage of the total fluorescence collected from all depths at that radius.

collected fluorescence decreased by 57% for broad-field excitation with epi-illumination, 73% for broad field excitation with transillumination, 49% for laser scanner excitation with epi-illumination, and 63% for laser scanner excitation with transillumination.

In simulations already described, the amount of collected fluorescence (expressed as a percentage of the weight of excitation photons incident on the tissue surface within the recording radius) was consistently greater for the laser scanner

Table 1 Intensity of fluorescence measured with transillumination using a longpass 530 nm filter.

	di-4ANEPPS-Stained Slice Facing Laser	di-4ANEPPS-Stained Slice Facing Away from Laser
Control	1 ± 0	0.67 ± 0.01
Fluorescence absorber	0.66 ± 0.16 ^a	0.53 ± 0.13 ^b

Values [mean ± (SD) standard deviation] are normalized to the control value with di-4ANEPPS-stained slice facing laser.

^ap < 0.05

^bp = NS for value in row 2 versus the value above it, paired 1-tail t test, n = 3.

excitation method compared with the broad-field method. With the threefold increased fluorescence absorption coefficient, it was greater by a factor of 6.8 times for epi-illumination and 10 times for transillumination. With the threefold increased excitation light absorption coefficient, the factor became 10.5 times for epi-illumination and 20 times for transillumination.

To further study the effects of variations in the absorption coefficient at 488 and 669 nm, we examined the depth of interrogation for a range of absorption coefficients that encompass normal values in myocardium stained with di-4-ANEPPS (Figs. 8 and 9). When the absorption coefficient of the fluorescence was increased (Fig. 8), the depth of interrogation decreased for epi-illumination (empty diamonds), while it increased for transillumination (filled squares). When the absorption coefficient of the excitation light was increased (Fig. 9), the depth of interrogation usually decreased.

3.3 Experimental Measurements

To test whether model predictions apply to optical measurements in heart tissue, we measured the contributions at two different depths to the collected fluorescence using differently stained tissue slices. We chose to examine the addition of a fluorescence absorber with transillumination because these conditions produced the greatest interrogated depth in our models.

For the slices that had no coloaded absorber (Tables 1 and 2, control), fluorescence intensity when the slice stained with di-4-ANEPPS faced away from the laser was 0.67 to 0.68 of

Table 2 Intensity of fluorescence measured with transillumination using a bandpass 670 ± 6 nm filter.

	di-4ANEPPS-Stained Slice Facing Laser	di-4ANEPPS-Stained Slice Facing Away from Laser
Control	1 ± 0	0.68 ± 0.08
Fluorescence absorber	0.5 ± 0.12 ^a	0.45 ± 0.09 ^b

Values (mean ± SD) are normalized to the control value with di-4ANEPPS-stained slice facing laser.

^ap < 0.05

^bp = NS for value in row 2 versus the value above it, paired 1-tail t test, n = 3.

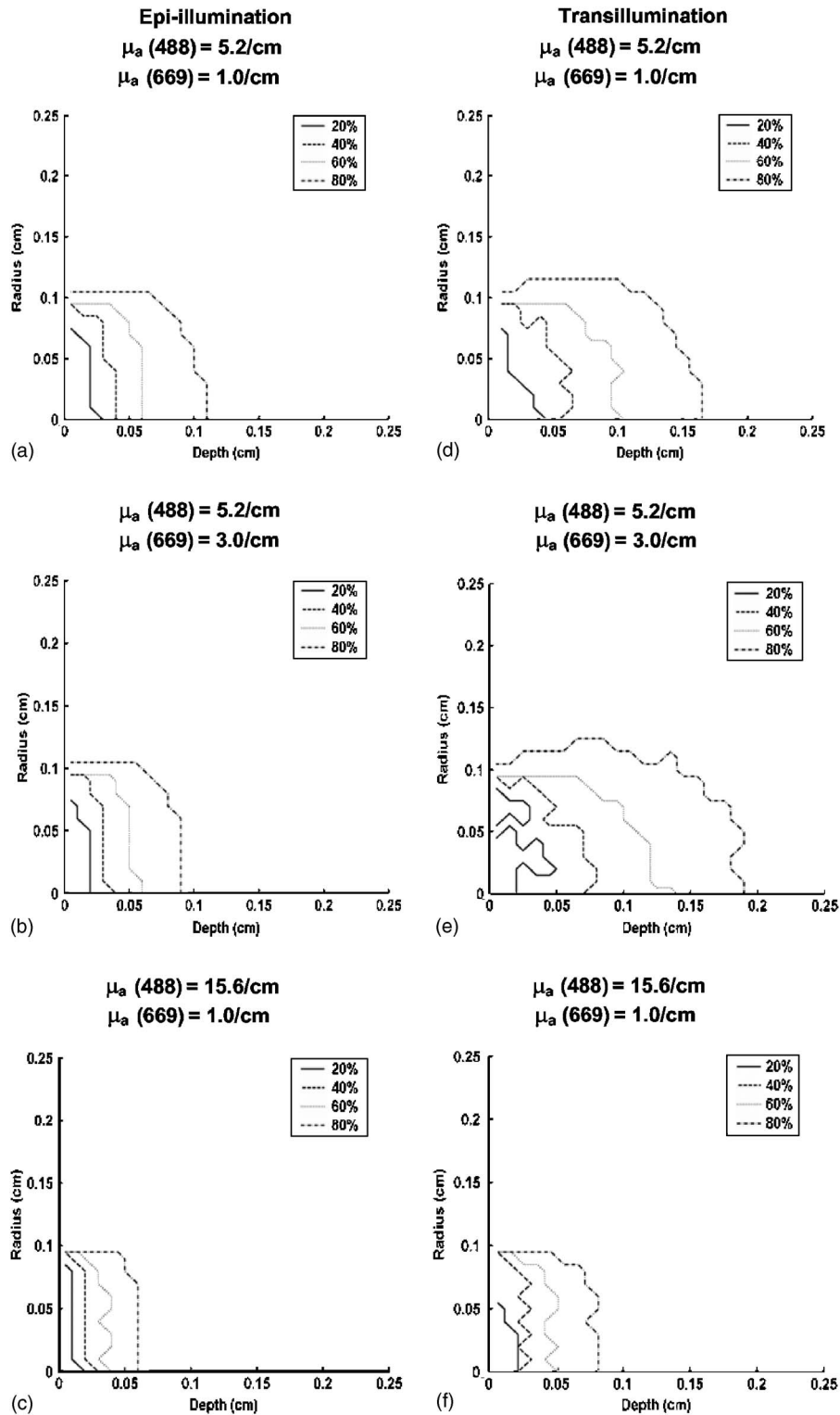


Fig. 6 Interrogated regions inside tissue for laser scanner excitation method with normal and threefold increase in absorption coefficients for excitation and fluorescence light wavelengths. Illumination radius was 0.1 cm. The region enclosed by each contour contains the originating sites of the collected photons having the greatest weights and whose summed weight was 20, 40, 60, or 80% of the total for all collected photons. Left column shows results for epi-illumination with (a) normal conditions, (b) effect of threefold increase in the absorption coefficient for the fluorescent wavelength, and (c) effect of threefold increase in the absorption coefficient for the excitation wavelength. Right column shows corresponding results for transillumination.

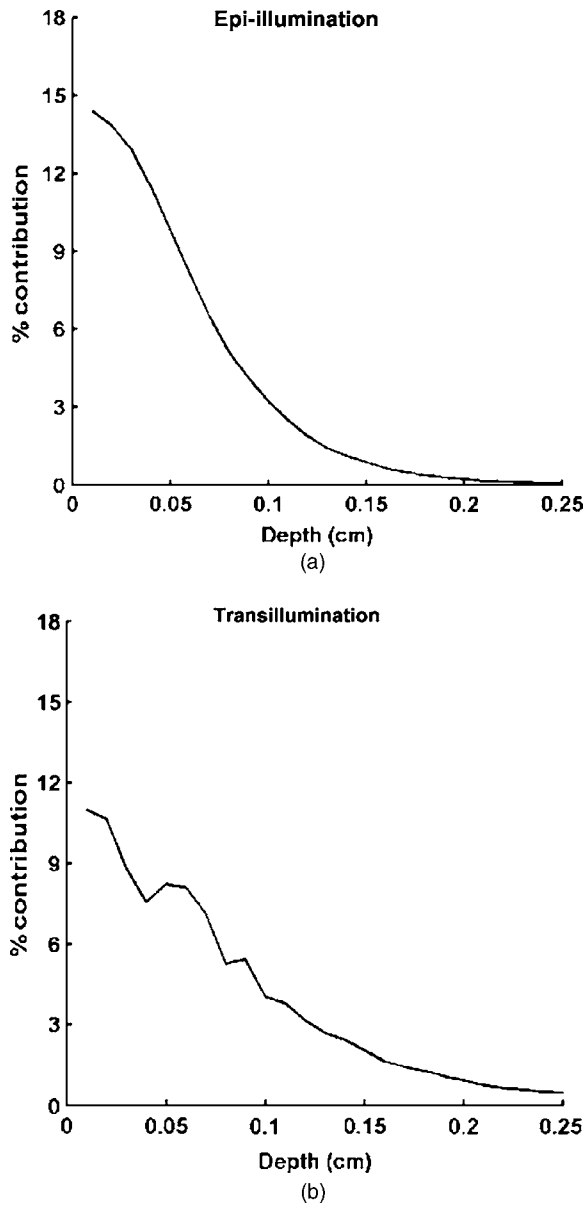


Fig. 7 Fluorescence contributions from different depths at a radius of 0.01 cm inside the tissue with normal optical properties for the laser scanner excitation method with results for (a) epi-illumination and (b) transillumination. The simulation was same as in Figs. 6(a) and 6(d). Fluorescence contribution from each depth was expressed as a percentage of the total fluorescence collected from all depths at that radius.

the value found when the slice faced the laser. With the fluorescence absorber coloaded, fluorescence intensities decreased for both positions of the slice containing the di-4ANEPPS. This can be seen by comparing row 1 with row 2 in Tables 1 and 2. However for both fluorescence filters tested, the decrease was smaller when the slice containing di-4-ANEPPS faced away from the laser, representing deeper tissue (from mean values of 0.67 to 0.53 in Table 1 and from 0.68 to 0.45 in Table 2, which are decreases of 21 and 34%, respectively) compared to the result found when the slice containing di-4ANEPPS faced the laser (from 1 to 0.66 in Table 1 and from 1 to 0.50 in Table 2, which are decreases of 34 and 50%).

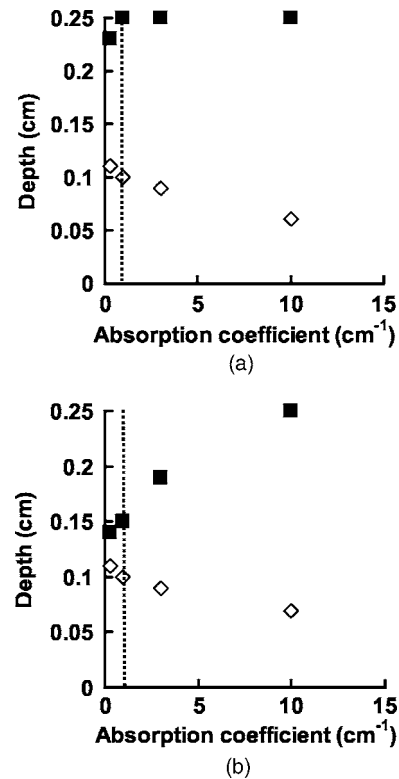


Fig. 8 Maximum depth of the tissue from which the brightest 80% of the fluorescence photons originated at a radius of 0.05 cm. Simulations used different absorption coefficients for fluorescence light. Results are shown for (a) broad-field and (b) laser scanner excitation methods, with absorption coefficients of 0.3, 1, 3, and 10/cm. Each panel shows results for epi-illumination (open diamonds) and transillumination (filled squares). The vertical dotted line indicates normal absorption coefficient for cardiac tissue stained with di-4-ANEPPS. A depth of zero corresponds to the tissue surface nearer the incident excitation light, and a depth of 0.25 cm corresponds to the tissue surface away from the incident excitation light.

These results indicate that the coloaded fluorescence absorber increased the relative contribution of the deeper slice to the collected fluorescence.

4 Discussion

A major limitation of conventional optical mapping in hearts stained with transmembrane voltage-sensitive fluorescent dyes has been the inability to map three-dimensionally in the heart. Novel optical mapping methods such as transillumination may overcome this. Knowledge of the size and depth of the tissue that is interrogated for a given method would be helpful in selecting a method. Here, we used 3-D Monte Carlo models to assess the interrogated regions in hearts stained with di-4-ANEPPS for the methods of transillumination and epi-illumination with either broad-field or laser scanner excitation. For each of these, we examined effects of coloaded the tissue with dyes that alter absorption at excitation and fluorescence wavelengths to modify the interrogated tissue size and depth.

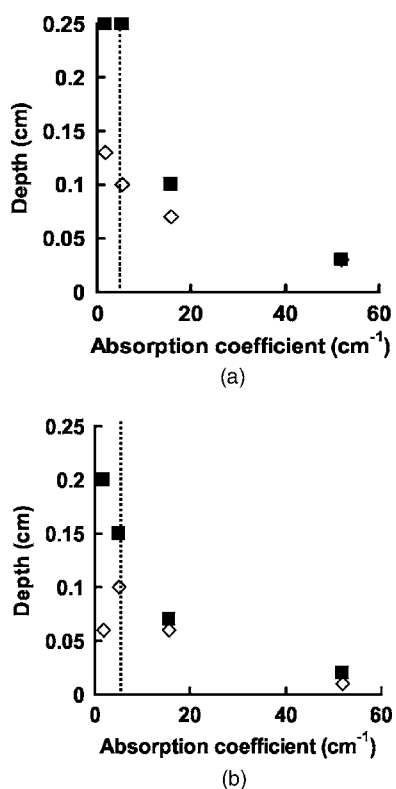


Fig. 9 Maximum depth of the tissue from which the brightest 80% of the fluorescence photons originated at a radius of 0.05 cm. Simulations used different absorption coefficients for excitation light. Results are shown for (a) broad-field and (b) laser scanner excitation methods, with absorption coefficients of 1.8, 5.2, 15.6, and 52/cm. Each panel shows results for epi-illumination (open diamonds) and transillumination (filled squares). The vertical dotted line indicates normal absorption coefficient for cardiac tissue stained with di-4-ANEPPS. A depth of zero corresponds to the tissue surface nearer the incident excitation light and a depth of 0.25 cm corresponds to the tissue surface away from the incident excitation light. Data points for epi-illumination and transillumination with an absorption coefficient of 52/cm in (a) are superimposed.

4.1 Interrogation Depth

The interrogated region for transillumination was deeper than that for epi-illumination (Figs. 4 and 6). Deeper interrogation may occur with transillumination because the length of the path traveled by the photon and attenuation may be greater for those fluorescence photons launched near the illuminated surface, enabling other fluorescence photons launched deeper in the tissue to contribute a greater percentage to the total collected fluorescence. This result is consistent with conclusions from a 1-D model.³ We also found the depth for transillumination was smaller with the laser scanner excitation method compared with the broad-field method, which may be due to differences in the excitation fluence distribution as well as the fluorescence collection. The excitation fluence for a narrow laser beam might attenuate more rapidly with depth due to lateral travel of scattered photons.

Results indicate an increase of absorption coefficient of the fluorescence light increased the depth of interrogation for transillumination (Figs. 4(e) versus 4(d) and Figs. 6(e) versus 6(d)), while it decreased depth for epi-illumination [Figs. 4(b)

versus 4(a) and Figs. 6(b) versus 6(a)]. This suggests cardiac optical mapping of tissue coloaded with a fluorescence absorbing dye would help to localize interrogation either near the illuminated surface for epi-illumination or deeper in the tissue for transillumination. Our results indicate such coloaded is possible by adding a blue dye to cardiac bathing solution.

An increase in absorption coefficient of the excitation light decreased depth of interrogation for all methods tested [Figs. 4(c) versus 4(a), Figs. 4(f) versus 4(d), Figs. 6(c) versus 6(a), and Figs. 6(f) versus 6(d)]. This suggests coloaded the heart with a red dye may be useful to localize interrogation near the illuminated surface for epi-illumination. However, this would not enhance the interrogation depth for transillumination.

4.2 Experimental Measurements

Predicted effects of coloaded with a fluorescence absorber are supported by experimental measurements. When the fluorescence absorber was coloaded, we found the collected fluorescence intensity decreased in our measurements with the di-4-ANEPPS slice away from or facing the laser to represent deeper and shallower tissue, respectively (Tables 1 and 2). This is comparable to the 47 to 63% decrease in the total weight of collected fluorescence produced by increasing the absorption coefficient for 669-nm light threefold in our Monte Carlo models for transillumination using the broad-field and laser scanner methods. While the similarity suggests we produced similar changes in absorption in the model and experiments, the amount of decrease will depend on the amount of fluorescence-absorbing dye added experimentally or the absorption coefficient in a model.

For the control data, the contribution of the deeper slice (i.e., measurement with di-4-ANEPPS away from the laser) was 67 to 68% of the contribution of the shallow slice (di-4-ANEPPS facing the laser). A smaller contribution of deeper tissue is consistent with the models for transillumination with broad-field and laser scanner excitation in which the interrogated region was primarily in the tissue nearer the illuminated surface representing shallow tissue [Figs. 4(d) and 6(d)]. With a fluorescence absorber coloaded, the contribution of the deeper slice was still less than the contribution of the shallow slice, consistent with the model results in which the interrogated region remained closer to the illuminated surface [80% contour in Fig. 4(e) and all contours in Fig. 6(e)]. However, with the coloaded absorber, the fluorescence intensity when the slice stained with di-4-ANEPPS faced away from the laser was 80 to 90% (column 2 versus 1, row 2, of both tables) of the intensity found when the slice faced the laser, whereas the corresponding values were only approximately 68% in the control data (column 2 versus 1, row 1 of both tables). This agrees with the relative increase in depth of interrogation in the models with the addition of the fluorescence absorber [compare Figs. 4(e) versus 4(d) and Figs. 6(e) versus 6(d)].

4.3 Absorbed Excitation Light

The predicted 83 to 84% of excitation photons absorbed in the heart tissue stained with di-4-ANEPPS in our models is largely accounted for by the absorption coefficient for excitation light in the tissue. For example, given the absorption coefficient of 5.2/cm at 488 nm, ignoring scattering, the ex-

ponential law of absorption would indicate 73% of the excitation light is absorbed over a photon pathlength of 0.25 cm. By accounting for additional distance of travel due to scattering, the Monte Carlo models are expected to absorb a greater percentage.

An increased absorption coefficient of excitation light produced a rise in the total amount of excitation light absorbed to approximately 94%, which is less than the rise expected from the absorption alone (with an absorption coefficient of 15.6/cm and a pathlength of 0.25 cm, ignoring scattering, the exponential law predicts 98% of the light is absorbed). The lower value in our Monte Carlo models may be due to effects of loss of photons by backscattering near the illuminated surface, which may prevent the value from approaching 100%.

4.4 Collected Fluorescence

An increase in the absorption coefficient for the fluorescence decreased the total weight of fluorescence collected by 25 to 63% for the four methods modeled. This was most pronounced for transillumination with the laser scanner excitation method. A decrease for the transillumination can be expected, given that some fluorescence photons that exit the far side of the tissue will have a longer travel distance and hence more chance to become absorbed in the tissue compared with photons that exit the illuminated surface.

The finding that an increased absorption coefficient for either excitation light or fluorescence decreased the total collected fluorescence intensity indicates the fluorescence light detector must be more sensitive when an absorber is used. For example, in all of our models with a threefold increase in the absorption coefficient for excitation light or fluorescence, we found the total weights of collected fluorescence decreased by 25 to 73%. This predicts, in the worst case for the 0.25-cm thickness modeled, the sensitivity of the detector must increase approximately fourfold to produce the same output signal level found without co-loading an absorber. This increase can be achieved by additional electron gain or transconductance amplification with photomultiplier tubes or photodiodes. Also the intensity of the incident excitation light can be increased if needed to produce more fluorescence. A small fluorescence intensity may become a more important limitation of transillumination for cases in which tissue thickness or absorption are greater than those in our models.

4.5 Lateral Interrogation

While results from a single radius at various depths (Figs. 5 and 7) are similar to Fig. 7 of Baxter et al.,³ our results also show lateral distributions of interrogated regions. The width of interrogation due to photon scattering inside the tissue is greater for transillumination compared with epi-illumination (most notably for the broad-field excitation method, e.g., Fig. 4). This is consistent with more scattering events for the transillumination, since fluorescence photons may travel greater distances before exiting the tissue. Also Fig. 4 shows that the radius of interrogation for the broad-field excitation is sensitive to changes in absorption coefficients.

Interestingly, the interrogated regions differ from results obtained with other metrics of spatial resolution. Estimates of lateral resolution as simply the imaging array element size divided by the magnification underestimate the interrogated

region. This underestimation has been attributed to scatter of photons within the tissue and is expected to prolong the action potential upstroke even if a very small area of the surface is imaged.^{5,6,13} Also, the distribution of fluorescence exiting the tissue surface that originates from a point source in tissue at a given distance from the surface is identical for subsurface imaging compared with transillumination [e.g., Figs. 2(a)—2(c) of Ref. 14].

4.6 Implications for Cardiac Optical Mapping

Electrophysiological studies that would benefit from mapping inside cardiac tissue include experiments with conduction block, fibrillation, regional ischemia, and electrical defibrillation.^{3,4,15,16} Of the methods analyzed here, results indicate broad-field excitation with transillumination and co-loading of a fluorescence absorber [Fig. 4(e)] provides the deepest interrogation. However, the increased range of tissue depths included in an interrogated region with transillumination is a limitation for studies of action potential upstroke velocity to assess rapid inward sodium current, microreentry, or defibrillation-shock-induced transmembrane potential changes on a microscopic spatial scale. Of all the methods analyzed, the smallest range of depths in an interrogated region was found with epi-illumination using the laser scanner method and addition of an excitation light absorber [Fig. 6(c)]. This may be useful in studies that require surface mapping with a smaller depth.

Acknowledgments

Supported by National Institutes of Health Grants HL52003 and HL67728, and American Heart Association Grant No. 0355805U.

References

1. M. S. Spach, P. C. Dolber, and P. A. W. Anderson, "Multiple regional differences in cellular properties that regulate repolarization and contraction in the right atrium of adult and newborn dogs," *Circ. Res.* **65**(6), 1594–1611 (1989).
2. I. R. Efimov, D. T. Huang, J. M. Rendt, and G. Salama, "Optical mapping of repolarization and refractoriness from intact hearts," *Circulation* **90**(3), 1469–1480 (1994).
3. W. T. Baxter, S. F. Mironov, A. V. Zaitsev, J. Jalife, and A. M. Pertsov, "Visualizing excitation waves inside cardiac muscle using transillumination," *Biophys. J.* **80**, 516–530 (2001).
4. S. B. Knisley, "Transmembrane voltage changes during unipolar stimulation of rabbit ventricle," *Circ. Res.* **77**(6), 1229–1239 (1995).
5. D. S. Rosenbaum, "Optical mapping of cardiac excitation and arrhythmias: a primer," in *Optical Mapping of Cardiac Excitation and Arrhythmias*, D. S. Rosenbaum and J. Jalife, Eds., pp. 2–7, Futura, Armonk, NY (2001).
6. L. Ding, R. Splinter, and S. B. Knisley, "Quantifying spatial localization of optical mapping using Monte Carlo simulations," *IEEE Trans. Biomed. Eng.* **48**, 1098–1107 (2001).
7. L. Wang, S. L. Jacques, and L. Zheng, "MCML—Monte Carlo modeling of light transport in multi-layered tissues," *Comput. Methods Programs Biomed.* **47**(2), 131–146 (1995).
8. V. K. Ramshesh and S. B. Knisley, "Spatial localization of cardiac optical mapping with multiphoton excitation," *J. Biomed. Opt.* **8**(2), 253–259 (2003).
9. A. Fischer, C. Cremer, and E. H. K. Stelzer, "Fluorescence of coumarins and xanthenes after two-photon absorption with a pulsed titanium-sapphire laser," *Appl. Opt.* **34**(12), 1989–2003 (1995).
10. E. Fluhler, V. G. Burnham, and L. M. Loew, "Spectra, membrane binding, and potentiometric responses of new charge shift probes," *Biochemistry* **24**, 5749–5755 (1985).
11. R. P. Haugland, *Handbook of Fluorescent Probes and Research Prod-*

- ucts*, 9th ed., Molecular Probes, Inc., Eugene, OR (2002).
12. D. T. Delpy, M. Cope, P. van der Zee, S. Arridge, S. Wray, and J. Wyatt, "Estimation of optical pathlength through tissue from direct time of flight measurement," *Phys. Med. Biol.* **33**, 1433–1442 (1988).
 13. C. J. Hyatt, S. F. Mironov, F. J. Vetter, C. W. Zemlin, and A. M. Pertsov, "Optical action potential upstroke morphology reveals near-surface transmural propagation direction," *Circ. Res.* **97**, 277–284 (2005).
 14. O. Bernus, M. Wellner, S. F. Mironov, and A. M. Pertsov, "Simulation of voltage-sensitive optical signals in three-dimensional slabs of cardiac tissue: application to transillumination and coaxial imaging methods," *Phys. Med. Biol.* **50**, 215–229 (2005).
 15. I. R. Efimov, Y. Cheng, D. V. Wagoner, T. Mazgalev, and P. Tchou, "Virtual electrode-induced phase singularity: a basic mechanism of defibrillation failure," *Circ. Res.* **82**(8), 918–925 (1998).
 16. M. J. Janse, F. J. L. van Capelle, H. Morsink, A. G. Kléber, F. Wilms-Schopman, R. Cardinal, C. N. d'Alnoncourt, and D. Durrer, "Flow of 'injury' current and patterns of excitation during early ventricular arrhythmias in acute regional myocardial ischemia in isolated porcine and canine hearts: evidence for two different arrhythmogenic mechanisms," *Circ. Res.* **47**(2), 151–165 (1980).